Journal of Materials Chemistry A

Interfacial defect passivation via imidazolium bromide for efficient, stable perovskite solar cells

Journal:	*Journal of Materials Chemistry A*
Manuscript ID	TA-ART-03-2024-001872.R1
Article Type:	Paper
Date Submitted by the Author:	17-May-2024

Complete List of Authors:	Chen, Zijing; Beijing National Laboratory of Condensed Matter Physics; University of the Chinese Academy of Sciences School of Physical Sciences, Jiang, Shiyu; Beijing National Laboratory of Condensed Matter Physics; University of the Chinese Academy of Sciences School of Physical Sciences, Liu, Zhenghao; Beijing National Laboratory of Condensed Matter Physics; University of the Chinese Academy of Sciences College of Material Sciences and Opto Electronic Technology Li, Yiming; Beijing National Laboratory of Condensed Matter Physics Shi, Jiangjian; Beijing National Laboratory of Condensed Matter Physics Wu, Huijue; Beijing National Laboratory of Condensed Matter Physics Luo, Yanhong; Beijing National Laboratory of Condensed Matter Physics; University of the Chinese Academy of Sciences School of Physical Sciences; Songshan Lake Materials Laboratory Li, Dongmei; Beijing National Laboratory of Condensed Matter Physics; University of the Chinese Academy of Sciences School of Physical Sciences, ; Songshan Lake Materials Laboratory Meng, Qingbo; Beijing National Laboratory of Condensed Matter Physics; University of the Chinese Academy of Sciences College of Material Sciences and Opto Electronic Technology; Songshan Lake Materials Laboratory

ARTICLE

Interfacial defect passivation via imidazolium bromide for efficient, stable perovskite solar cells

Received 00th January 20xx,
Accepted 00th January 20xx

DOI: 10.1039/x0xx00000x

Zijing Chen,[a,c] Shiyu Jiang,[a,c] Zhenghao Liu,[a,b] Yiming Li,*[a] Jiangjian Shi,[a] Huijue Wu,[a] Yanhong luo,[a,c,d] Dongmei Li,*[a,c,d] Qingbo Meng*[a,b,d]

In this respect, 1-methy-3-benzyl-imidazolium halides (BzMIMX, X= I, Br, Cl) have been introduced to passivate the $FAPbI_3$/spiro-OMeTAD interface for efficient and stable PSCs. And the BzMIMBr exhibits the best passivation effect, which Br^- ions can well passivate the iodide vacancy from the perovskite surface, and in the meantime, the weak coordination interaction between N atoms from imidazole and Pb^{2+} cations also passivate under-coordinated Pb^{2+} and reduce interfacial defects in some degree. Interestingly, very small amount of the BzMIMBr could penetrate the bulk perovskite to further passivate grain boundaries of the bulk perovskite film. The champion PCE of our small-size PSC devices can reach 25.3% with negligible hysteresis. Besides, π-π self-assembly from the $BzMIM^+$ can strength the interfacial modification effect, which enhances the anti-humidity ability of perovskite films and the devices. When being stored at ambient condition (20°C and 20%RH) over 5,000 h, this modification helps the cell to maintain 90% of its initial efficiency, indicating its good long-term stability. And BzMIMBr modified devices exhibit much better operational stability by maintaining 91% of the initial efficiency after 1000 h continuous illumination with a bias voltage near maximum power point. This osmotic modification strategy provides a feasible way to realize high performance and stable PSCs.

Introduction

Over the past decade development, the certified power conversion efficiency (PCE) of hybrid perovskite solar cells (PSCs) has already exceeded 26%,[1-3] however, the stability of PSCs is still a severe limitation to industrialization and practical application.[4] As the PSC is a kind of photovoltaic devices with typical layered structure, defects from hetero-interfaces are undoubtedly the major stumbling block to further improving the cell performance,[5] especially stability issues.[6] Deep understanding interface-related physical processes is particularly important to realize optimal interface design and develop effective passivation methods or materials for efficient devices. In fact, to solution-processed perovskite layers, faster crystallization rate easily brings about defects derived from structural disorder,[1, 7] including lattice defects[8] and grain boundary defects in the bulk[9, 10] or the surface of the perovskite absorber.[11] Some researches demonstrated that the carrier lifetime at the grain boundary is one order of magnitude lower than that of the perovskite film itself.[12-14] Moreover, once perovskite-related interfaces are deteriorated, it will result in unsatisfied cell performance and poor stability.[15, 16] Therefore, developing interface passivation techniques is an effective strategy to reduce non-radiative recombination,[17-19] improve interface properties[20] and enhance the photoelectric efficiency and stability of PSCs.[21]

Surface passivation toward perovskite films is widely used to eliminate interfacial defects (lattice vacancies[22, 23] and uncoordinated ions,[24] etc.),[25] improve interfacial carrier transportation[26] and hydrophobicity.[27, 28] Different kinds of surface passivation materials have been explored, including Lewis acid/base[29, 30] (*e.g.* DMSO[31]), organic halide salts (*e.g.* PEAI[32]), polymers (*e.g.* polystyrene (PS),[33] polymethyl methacrylate (PMMA) [34]), fullerenes[35] and their derivatives (e.g. PCBM,[36] PCBA[37, 38]). However, most of these passivators have poor electrical conductivity, detrimental to charge transportation at the interface. Besides, some materials with larger molecular structures (fullerenes and their derivatives) tend to have poor orientation at the interface, which has a negative effect on the reproducibility of the device.[39] Obviously, further exploring more effective interface passivation materials is also an important topic to efficient and stable PSCs. Imidazolium derivatives as additives into PSCs exhibited attractive advantages. For example, ionic radius of imidazolium cations can be tailored by selecting alkyl groups to satisfy the limit of tolerance factor,[40] as a result, introducing imidazolium cation into the bulk perovskite layer was supposed to regulate

[a] *Beijing National Laboratory for Condensed Matter Physics, Key laboratory for Renewable Energy (CAS), Institute of Physics, Chinese Academy of Sciences (CAS), Beijing 100190, P. R. China.*
[b] *Centre of Materials Science and Optoelectronics Engineering, University of Chinese Academy of Sciences, Beijing 100049, P. R. China*
[c] *School of Physical Sciences, University of Chinese Academy of Sciences Beijing 100049, P. R. China.*
[d] *Songshan Lake Materials Laboratory, Dongguan 523808, P. R. China*
† Electronic Supplementary Information (ESI) available: Additional figures. See DOI: 10.1039/x0xx00000x
* Corresponding authors.
E-mail addresses: qbmeng@iphy.ac.cn (Q. Meng), liyiming4869@iphy.ac.cn (Y. Li), dmli@iphy.ac.cn (D. Li).

perovskite crystallization[41] and passivate defects.[42,43,44] Theoretically, imidazole derivatives are also suitable for interface treatment due to the above superiority,[45] however, related researches have been seldom reported.

Here, 1-methy-3-benzyl-imidazolium halides (BzMIMX, X= I, Br, Cl) have been introduced to passivate the $FAPbI_3$/spiro-OMeTAD interface for efficient PSCs. Among the three BzMIMX, the BzMIMBr exhibits the best passivation effect. It is found that, the Br^- ions can well passivate the iodide vacancy from the perovskite surface, meanwhile, the weak coordination interaction between N atoms from imidazole and Pb^{2+} cations may also passivate under-coordinated Pb^{2+} and reduce interfacial defects. More interesting, a slight amount of the BzMIMBr could penetrate the bulk perovskite, which further passivates grain boundaries of the bulk perovskite film. Besides, π-π self-assembly from the electron delocalization of $BzMIM^+$ can strength the interfacial modification effect, which further enhances anti-humidity ability of perovskite films and the devices. On this basis, the champion PCE of our small-size PSC devices can reach 25.3% with negligible hysteresis. And BzMIMBr modified devices exhibit much better operational stability by maintaining 91% of the initial efficiency after 1000 h continuous illumination with a bias voltage near maximum power point. When being stored at ambient condition (20°C and 20%RH) over 5,000 h, this modification helps the cell to maintain 90% of its initial efficiency, indicating its good long-term stability. This osmotic modification strategy provides a feasible way to realize high performance and stable PSCs.

Experimental

Reagents and materials

PbI_2 (99.99%), formamidinium iodide (FAI, 99%) and methylammonium chloride (MACl, 99%) were bought from Xi'an Polymer Light Technology Corp.. Tin (II) chloride dihydrate ($SnCl_2{\cdot}2H_2O$), urea and mercaptoacetic acid (TGA) were from Shanghai Aladdin Biochemical Technology Co. LTD.. Trichloromethane, isopropanol and alcohol were bought from Beijing Chemical Industry Group CO., LTD.. 1-methy-3-benzyl-imidazolium halides (BzMIMX, X= I, Br, Cl, 99.9%), Dimethyl sulphoxide (DMSO), N, N-dimethylformamide (DMF) and chlorobenzene (CB) were from Alfar Aesar. 4-tert-butylpyridine (TBP) and bis(trifluoromethane) sulfonimidelithium salt (LiTFSI) were bought from Sigma-Aldrich. [6,6]-phenyl-C_{61}-butyric acid methyl ester (PCBM), *spiro*-OMeTAD were purchased from Luminescence Technology Corp.. All the chemicals were directly used without further purification. Laser-patterned FTO glass (sheet resistance of 8.5 $\Omega{\cdot}sq^{-1}$) was sequentially cleaned with a mild detergent, alkali liquor, distilled water and ethanol in an ultrasonic bath. The substrate was treated with ozone for 15 min prior to use.

SnO_2 layers from chemical bath deposition (CBD) method

CBD solution was prepared by following the reference,[46] briefly, 275 mg $SnCl_2{\cdot}2H_2O$, 1.25 mL HCl, 1.25 g urea, 25 µL TGA were mixed in 100 mL deionized water. O_3-treated FTO substrates were immersed into the CBD solution. The solution was heated at 90°C for ~4 h. After the reaction, the substrate was removed from the solution and washed by deionized water and isopropanol sequentially in ultrasonic bath for 5 min each. As prepared SnO_2 layer was defined as CBD-SnO_2. Before use, CBD-SnO_2 layers were annealed in the air (25%~ 35%RH) at 170°C for 60 min, then UV-O_3 treated for 15 min.

Solar cell fabrication

Perovskite precursor solution was prepared by dissolving 1.73 M PbI_2, 1.6 M FAI and 0.53 M MACl in DMF/DMSO mixed solvent (v: v= 8: 1).[47-50] The precursor solution was stirred for 4 h and filtered before use. Perovskite films were fabricated by anti-solvent one-step spin-coating method.[51] In details, perovskite precursor solution was spin-coated at 1000 rpm for 10 s and subsequently at 5000 rpm for 30s, 120 µL CB was poured onto the spinning substrate at 15 s in the second spinning step. The perovskite film was heated at 100°C for 60 min in the air (~20% RH).[52, 53] For BzMIMX (X = Cl/Br/I) treated film, BzMIMX solution was prepared by dissolving 1.5 mg/mL BzMIMBr in trichloromethane. BzMIMX solution was spin-coated on the surface of $FAPbI_3$ perovskite films, subsequently annealed at 60ºC for 6 min. Average 200 nm-thickness *spiro*-OMeTAD layer with Li and Co-doped was deposited onto the perovskite film at 3000 rpm, then heated at 60°C for 8 min. Spin-coating processes of perovskite and *spiro*-OMeTAD layers were carried out in the glove box. At last, 80 nm-thickness Au electrode was deposited via thermal evaporation under the vacuum of 10^{-7} Torr.

Characterizations

If not special noting, all the measurements were carried out in the ambient condition (25°C, 20~30%RH). XPS measurement were performed on an ESCALAB 250Xi (Thermo Fisher) instrument. UV-vis absorption spectra were obtained on Shimadzu UV-2550. Steady-state and time-resolved transient photoluminescence (TRPL) spectra were performed on a PL spectrometer (FLS 900, Edinburgh Instruments), that is, the samples were excited at 444.6 nm from a picosecond pulsed diode laser (EPL-445) and measured at 728 nm. SEM images were measured by scanning electron microscopy (SEM, Hitachi S4800) under 10 kV at various magnifications. Atomic force microscope (AFM) images and kelvin probe force microscope (KPFM) image were carried out on MultiMode 8 SPM, and the surface potential of the tip was calibrated with Au reference (ψ_{Au}= 5.10 eV). Contact angles were obtained on OCA25, DataPhysics. Diffraction (XRD) patterns was measured on a Bruker D8 Advance diffractometer by using CuKα as the radiation source. Modulated transient photocurrent/ photovoltage (m-TPC/TPV) measurements were obtained by using our lab-made setup with a tunable nanosecond laser (Opotek, RADIANT 532 LD) pumped at 532 nm, recorded by a sub-nanosecond resolved digital oscilloscope (Tektronix, MDO3034) with input impedances of 50 Ω or 1 MΩ, respectively. A signal generator (Tektronix, AFG3052C) together with a low-pass filter was applied to give steady-state bias voltages over the cell. *J-V* characteristics were measured under AM 1.5 simulated sunlight (100 $mW{\cdot}cm^{-2}$) irradiation, Zolix SS150A, recorded on a digital source meter (Keithley model 2602), and light intensity for the *J-V* measurement was calibrated with a reference silicon cell.[54, 55] A black mask on solar cells was used to determine an aperture of 0.08912 cm^2 and the

area contacted with Au back is 0.162 cm^2. And the scanning speed was 50 mV s^{-1} with a delay time of 0.2 s. All the reverse scanning *J-V* curves are adopted unless otherwise noted. External quantum efficiency (EQE) spectra were performed by using Enli Technology (Taiwan) EQE system, which was calibrated with a crystalline silicon photovoltaic cell before use. "Double 60" stability testing of perovskite films (simultaneously at 60°C and 60%RH (relative humidity)) and "Double 85" stability testing of perovskite solar cells (simultaneously at 85°C and 85%RH) were performed in a temperature & humidity chamber (EYELA, KCL-1000). Here, the devics for 85°C heating testing were based on poly(3-hexylthiophene) (P3HT) instead of spiro-OMeTAD, in order to remove instability sources as soon as possible.

Results and discussion

In this work, $BzMIM^+$ with different anions X (X= I, Br, Cl) is used as interfacial materials toward perovskite surface. Its molecular structure is presented in Fig. 1a. Appropriate amount of 1-methyl-3-benzyl-imidazolium halides (BzMIMX, X= I, Br, Cl) in $CHCl_3$ solution was directly spin-coated on the surface of $FAPbI_3$ perovskite films, subsequently annealed at 60ºC for 6 min. Here, BzMIMBr is taken as an example for subsequent characterizations. For comparison, no extra treatment toward the perovskite film is defined as the control sample. Firstly, effect of BzMIMBr modification on the perovskite surface is studied by scanning electron microscopy (SEM). We can see from Fig. 1b that, some holes on the surface of the control film are observed, however, when the BzMIMBr is introduced on the perovskite film, the film surface is pin-hole free while its grain boundaries are filled with small white particles. Obviously, the BzMIMBr modification can bring about better surface coverage (Fig. 1c), which effectively reduces non-radiative recombination. However, this post-treatment basically does not change the perovskite grain sizes, according to statistic distribution results (Fig. S1, Supporting Information). Furthermore, surface characteristics of perovskite films have been analyzed by Kelvin probe force microscopy (KPFM) (Fig. 1d). For the modified perovskite, the half-peak full width (FWHM) of its contact potential difference (CPD) value is 15.0 mV, narrower than that of untreated perovskite films (25.0 mV). This means excellent uniformity of BzMIMBr modified perovskite films. As the surface potential of the probe was calibrated by Au film (Au= 5.10 eV), the surface potential of the unmodified and modified perovskite films is 770.5 and 1067.6 mV, respectively, indicating the BzMIMBr film is uniformly distributed on the perovskite surface and there is some chemical interaction between BzMIMBr and perovskite. Considering the possible impact of subsequent spin-coating spiro-OMeTAD solution on this interaction, we washed the perovskite/BzMIMBr film with chlorobenzene and repeated KPFM measurement. Uniform distribution of the BzMIMBr can be well kept with slight reduction in CPD (1067.6 vs. 981.1 mV) after chlorobenzene washing (Fig. S2). Comparatively, when the sample was directly washed with chloroform, it seems all the BzMIMBr has been washed away (Fig. S3). Obviously, this interaction between perovskite and BzMIMBr can be well maintained after the spiro-OMeTAD was deposited.

Based on the Owens-Wendt-Rabel-Kaelble (OWRK) method,

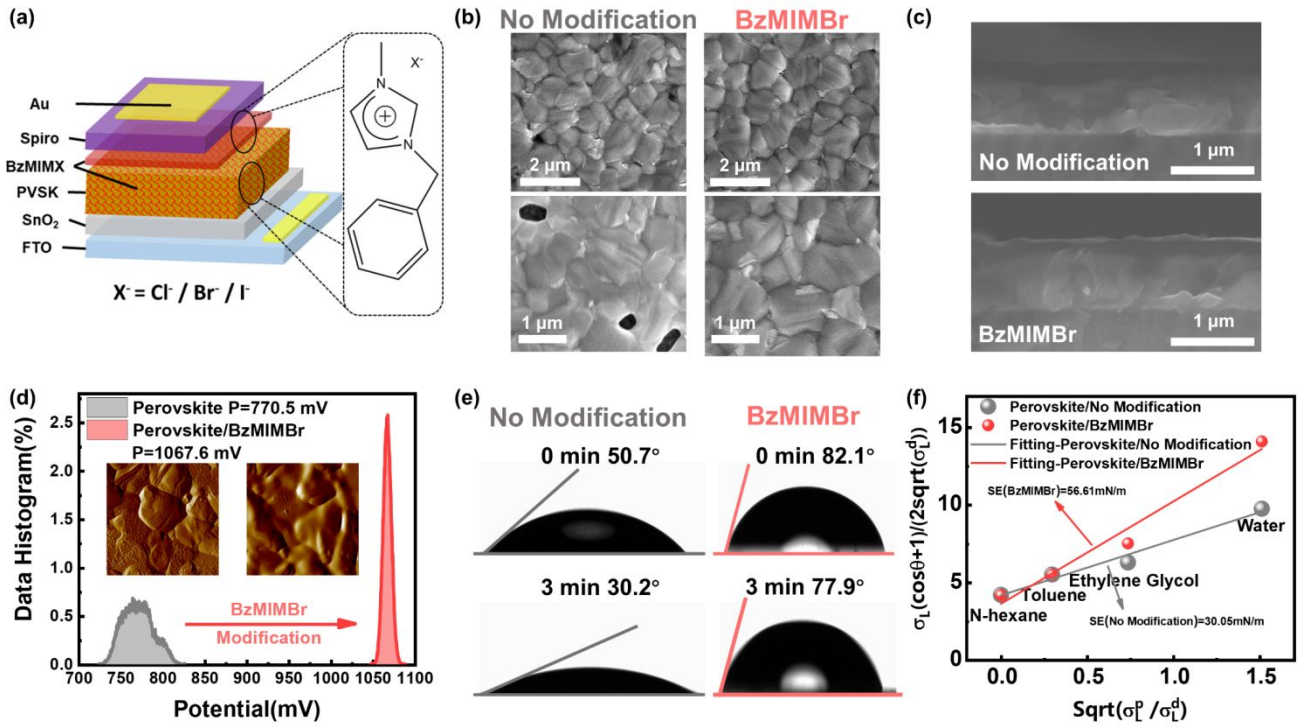

Fig. 1. (a) Schematic illustration of the PSC configuration together with molecular structure of BzMIMBr; (b) Top-view SEM images, (c) Cross-section SEM image of perovskite films with/without BzMIMBr. (d) Corresponding contacting potential difference distributions for perovskite films with/without BzMIMBr treatment. (e) Contact angle measurement and (f) surface energy measurement of perovskite films with/without BzMIMBr using the OWRK method.

we also carried out surface tension measurement to find out the effect of BzMIMBr modification on the hydrophobicity of perovskite films. As shown in Fig. 1e, the water contact angle of the untreated perovskite film decreases significantly from 50.7° (~ 0 s) to 30.2° after 3 min. However, when being treated by BzMIMBr, the perovskite film exhibits much higher water contact angle by reaching 82.1° (~ 0 s) and remaining 77.9° after 3 min. Obviously, the treated perovskite film has excellent moisture resistance. Besides, the contact angles (ϑ) of four solvents on the perovskite surface are also obtained, and corresponding surface energy is obtained from the relationship between ϑ and the tension properties of these solvents (Fig. 1e and Fig. S4). The moisture resistance of passivated perovskite films is mainly due to its high surface energy and dense distribution of the BzMIMBr on the perovskite surface, which will greatly improve the moisture stability of the device under high humidity environment. According to the absorption spectra, there is no significant difference in the band edge between the control and BzMIMBr-treated perovskite films, suggesting that BzMIMBr modification does not alter the bandgap of the perovskite film, however, the control exhibits relatively weak absorption below ~530 nm probably due to its poor crystal quality (Fig. S5).

On this basis, PSCs with the configuration of FTO/SnO_2/perovskite/modified layer/spiro-OMeTAD/Au were fabricated, which SnO_2 layer was derived from chemical bath deposition method, and the composition of the perovskite layer is $FAPbI_3$ (Fig. 1a). PCE statistical histograms of the four devices including three treatment materials are shown in Fig. 2a. We can see that, the control cell only exhibits an average PCE of 22.7% with 25.4 mA·cm^{-2} of the J_{SC}, 1.135 V of the V_{OC}, and 0.789 of the *FF*. When the BzMIMX are introduced, the average PCE increases from 23.4% (BzMIMI), 23.5% (BzMIMCl) to 24.7% (BzMIMBr) (Fig. 2a-b). Among the three imidazolium halides, the BzMIMBr exhibits the best interface modification ability. The improvement mainly lies in *FF* and V_{OC}. Furthermore, the optimal BzMIMBr concentration (1.5 mg/mL in chloroform) was also obtained, as shown in Fig. 2c and Fig. S6. The champion BzMIMBr modified cell exhibits the highest PCE of 25.3% with the J_{SC} of 25.77 mA cm^{-2}, the V_{OC} of 1.174 V, and the *FF* of 0.837 with negligible hysteresis (Fig. 2d). Furthermore, the BzMIMBr modified cell demonstrates a steady-state PCE of 24.4% at the maximum power-point (MPP), comparatively, the conventional cell without modification only gives a maximum PCE of 23.0%

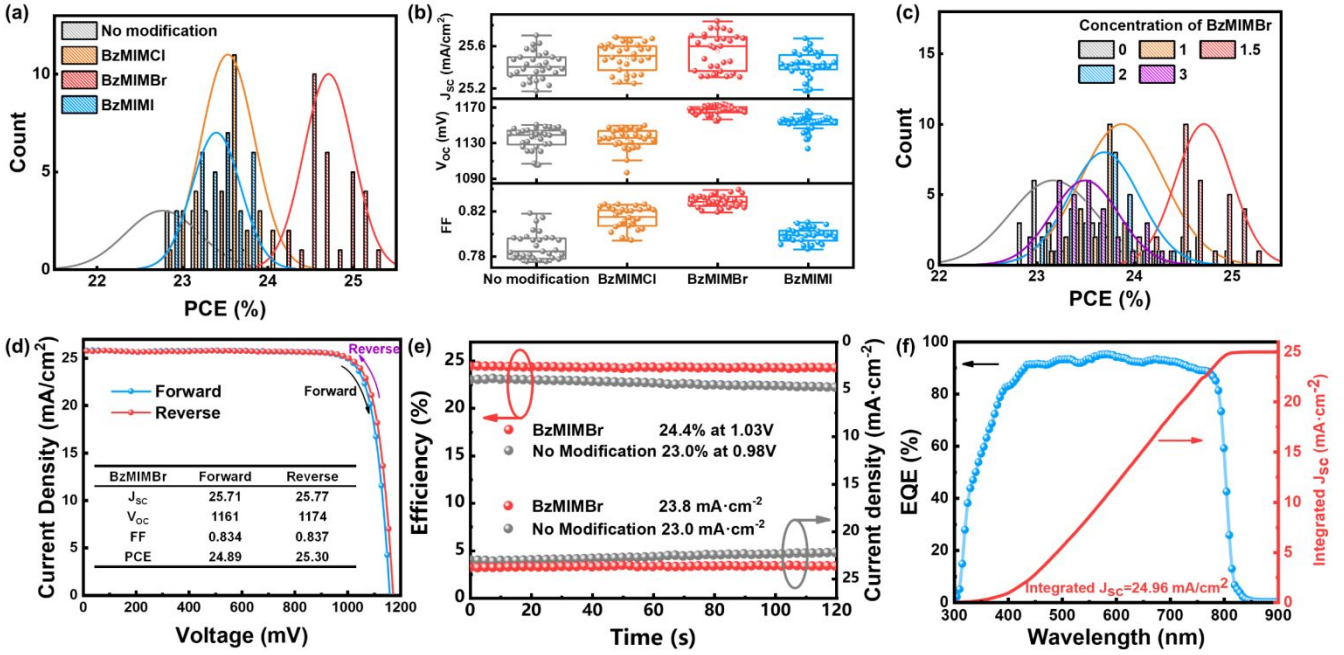

Fig. 2. (a) PCE distribution histograms of the cells with no modification and modifications by BzMIMCl, BzMIMBr and BzMIMI; (b) Detailed statistics of performance parameters; (c) PCE distribution histograms of the cells modified by BzMIMBr with different concentration; (d) Current density-voltage (*J-V*) characteristic curves of the typical cells with BzMIMBr; (e) Stabilized power output results under maximum power-point; (f) EQE and integrated current density spectra of the BzMIMBr cell.

(Fig. 2e). According to the external quantum efficiency (EQE) spectrum, the BzMIMBr cell presents an integrated current density of 24.96 mA·cm^{-2}, in good accordance with the experimental J_{SC} (Fig. 2f). This significant enhancement in device performance is attributed to our modification toward the perovskite/spiro-OMeTAD interface, which will be discussed below.

X-ray photoelectron spectroscopy (XPS) has been employed to explore the interaction between BzMIMBr and the perovskite (Fig. S7 and Fig. 3a-c). We can see that, when the BzMIMBr is introduced, all the peak positions of N1s and Br3d core levels

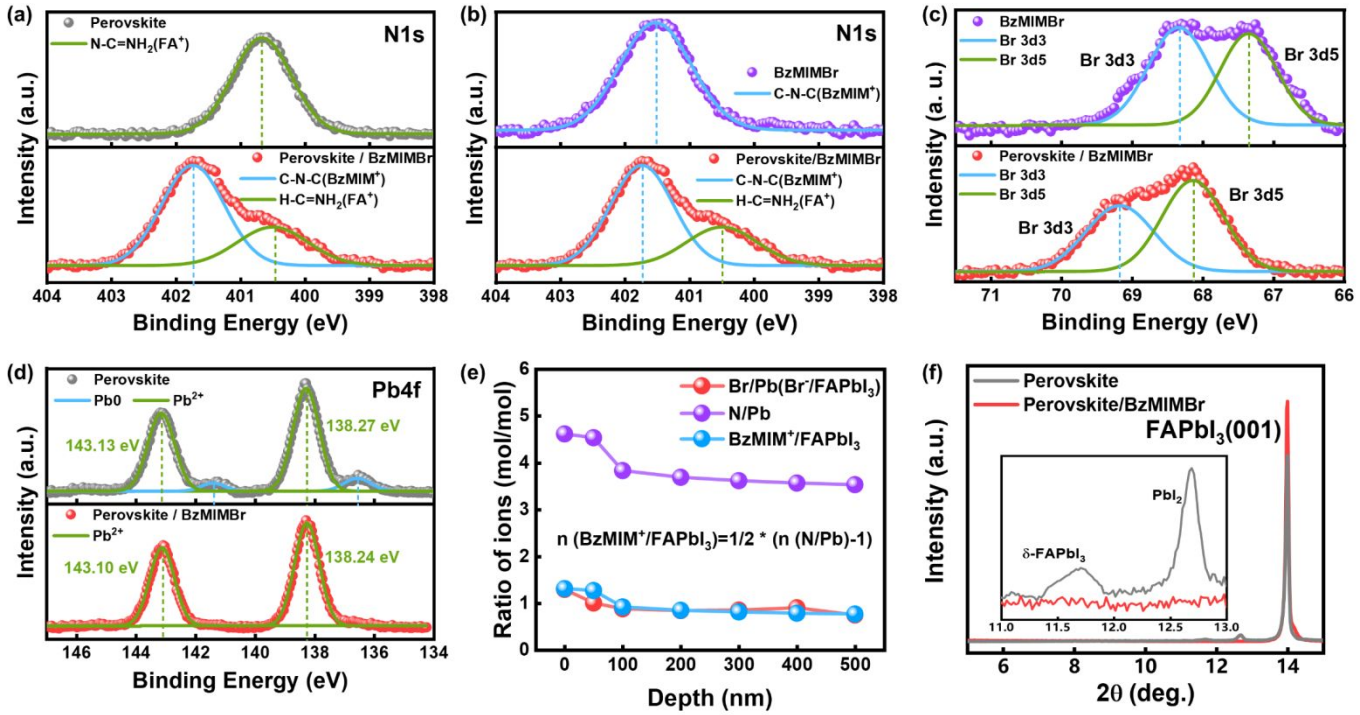

Fig. 3. XPS-spectra analysis of N1s core energy levels (a) in perovskite films with/without BzMIMBr; (b) in BzMIMBr film and Perovskite/BzMIMBr film, respectively; XPS-spectra analysis of (c) Br 3d3 and Br 3d5; (d) Pb 4f core energy levels in perovskite films with/without BzMIMBr; (e) XPS depth profile of Br and N elements in the perovskite film with/without BzMIMBr. (f) XRD of perovskite films with/without BzMIMBr.

are shifted slightly, which are closely related to the variation in chemical environments of these two elements (Fig. 3a-b). To the perovskite/BzMIMBr sample, its N1s spectrum is deconcolved into two peaks at 400.46 and 401.73 eV, corresponding to nitrogen from FA^+ and imidazolium, respectively. In comparison to the intrinsic $FAPbI_3$ and $BzMIM^+$, its N1s peak from FA^+ (400.67 eV) is slightly down-shifted, however, its N1s peak from the $BzMIM^+$ (401.52 eV) is slightly up-shifted instead, suggesting some interactions between $BzMIM^+$ and $FAPbI_3$ (Fig. 3a-b). That is, weak coordination interaction may occur between under-coordinated Pb^{2+} and N atom from $BzMIM^+$ (:$N(CH_3)$). Besides, by comparison of pure BzMIMBr sample, the downshift of $Br3d^3$ and $Br3d^5$ peaks also confirms Br^- ions occupy the V_I (iodide vacancy) positions to afford Pb-Br bond on the perovskite surface, which also leads to the two metallic Pb peaks centered at 141.36 and 136.54 eV disappeared completely (Fig. 3c-d, Fig. S8). However, for the Pb^{2+} cation, its Pb4f7/2 and Pb4f5/2 peak positions slightly change due to thimbleful Pb-Br bond formation [56]. As a result, BzMIMBr modification toward the $FAPbI_3$ perovskite is beneficial for passivating the V_I and suppressing Pb cluster formation. Depth-dependent XPS measurements are also performed (Fig. 3e). Considering Br and Pb are the characteristic elements of BzMIMBr ($C_{11}H_{13}BrN_2$) and $FAPbI_3$ ($CH_5N_2PbI_3$), respectively, the molar ratio of these two characteristic elements approximately reflects the relative content of Br^- at different depths of perovskite films (Fig. S9). On the perovskite surface (< 50 nm), there is higher BzMIMBr concentration, however, with the etching depth increasing, a small amount of Br^- ion can be found and Br^- ion distribution is basically homogeneous. Similar variation tendency of N1s XPS core is also obtained. This indicates that the BzMIMBr not only passivates the perovskite surface, but also penetrates the film inside and further passivate defects in the bulk. Furthermore, perovskite films before and after the BzMIMBr treatment are characterized by X-ray diffraction (XRD). In comparison to the pure BzMIMBr, the main diffraction peak at 14° is attributed to the black phase of $FAPbI_3$, no matter treated or not (Fig. S10).[57] To the untreated sample, its peak intensity is weaker than that of the BzMIMBr modified film, indicating its unsatisfied crystal quality, accompanied with PbI_2 residual (12.7°) and a little δ-phase $FAPbI_3$ (11.7°). After the BzMIMBr is introduced, these two impurities disappear, suggesting the BzMIMBr incorporation indeed can effectively prevent the $FAPbI_3$ decomposition and phase transition, meanwhile, no 2D perovskite with $BzMIM^+$ is found as well (Fig. 3f and Fig. S10).

As we know, defects in perovskite films will significantly affect the crystal quality of the perovskite. In order to investigate the influence of BzMIMBr incorporation on the electrical properties of the device, trap density (N_t) of perovskite films is evaluated by space charge limited current (SCLC) method based on an electronic device with the configuration of FTO/ETL/perovskite/BzMIMBr/PCBM/Au, as shown in Fig. 4a-b. The current increases linearly with the applied voltage until a kink point shows an ohmic response. Then, the current presents a rapid nonlinear increase when the applied voltage exceeds this kink point, due to the injected carrier filling the trap state. The voltage applied at the kinks is defined as the limiting voltage full of traps (V_{TFL}), which is used to estimate the trap state density.[40] Compared with unmodified devices, the V_{TFL} of BzMIMBr modified devices is reduced from 0.78 to 0.22 V, and corresponding defect density is reduced

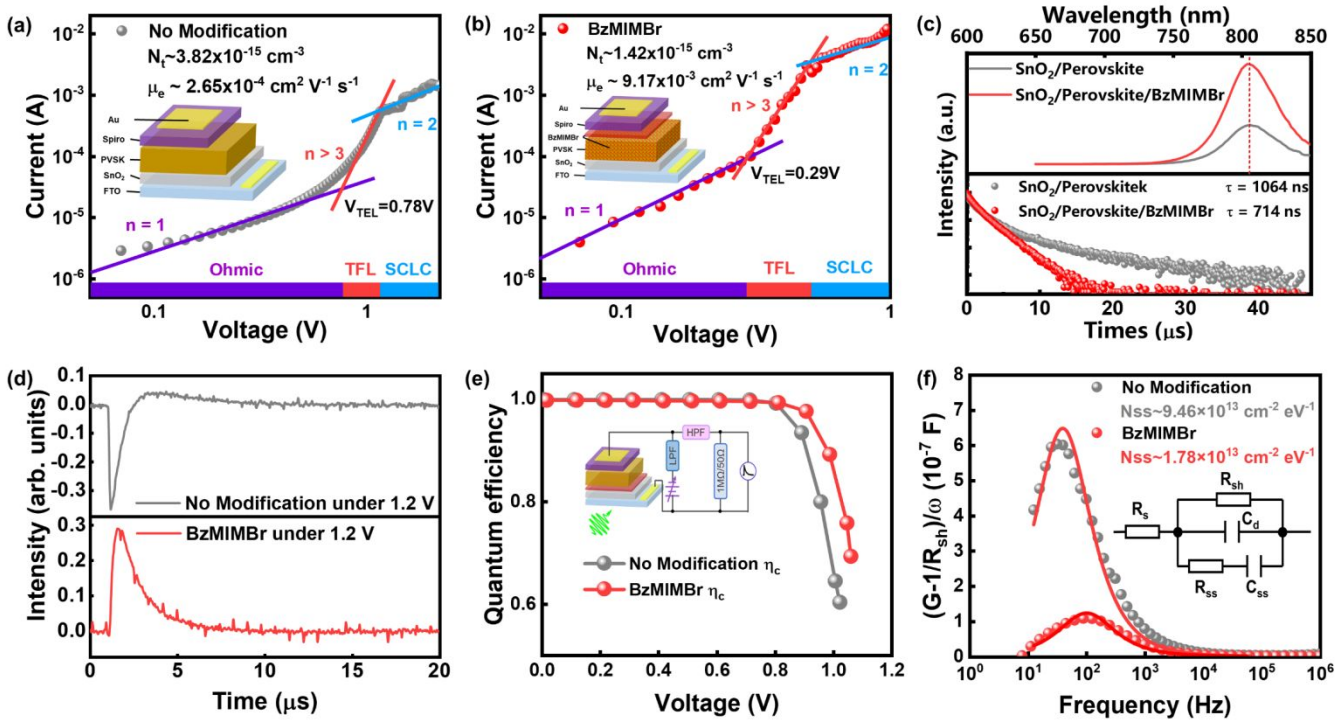

Fig. 4. Space charge limited current curves for electron-only devices (a) without and (b) with BzMIMBr modification; (c)Steady-state photoluminescence (PL) spectra and Time-resolved photoluminescence (TRPL) spectra of SnO_2/perovskite, SnO_2/perovskite/BzMIMBr interfaces; (d)Transient photocurrent curves of the cells under 1.2 V; (e)Voltage-dependent charge collection efficiency (η_C) of the cells measured from modulated electrical transient measurements; (f) Interface defect extraction of the cells by using admittance measurement.

from 3.82×10^{15} to 1.42×10^{15} cm^{-3}. And the electron mobility (μ_e) of as-prepared perovskite films is also estimated, that is, the μ_e of the BzMIMBr modified sample is 9.17 × 10^{-3} cm^2 V^{-1} s^{-1}, higher than that of the control sample (2.65 × 10^{-4} cm^2 V^{-1} s^{-1}). In addition, according to the steady-state PL and TRPL spectra, the carrier extraction ability of the perovskite/HTL interface is also affected by this interface modification. The carrier lifetime of SnO_2/untreated perovskite film (700 ns) is lower than that of SnO_2/perovskite/BzMIMBr films (1064 ns), indicating that the BzMIMBr has excellent defect passivation capability (Fig. 4c). This is in good agreement with the enhancement of the *FF* of the BzMIMBr modified cells.

Interface properties of devices have been researched by modulated transient photocurrent/photovoltage (m-TPC/TPV) technique and extended admittance characterization.[58, 59] Firstly, transient photocurrents under 1.2 V bias voltage are presented in Fig. 4d. At higher bias voltage, the BzMIMBr modified device exhibits better charge collection ability, indicating better inhibition toward non-radiative recombination. In the meantime, BzMIMBr modification successfully eliminates a strong negative signal at 1.2 V, suggesting smooth charge transportation in the perovskite film. Furthermore, the charge collection efficiency (η_C) at different bias voltages is derived from the decay lifetimes of TPC (τ_{TPC}) and TPV (τ_{TPV}) by following the Equation as η_C (V)= 1- τ_{TPC} (V)/τ_{TPV} (V) (Fig. S11-S14).[60, 61] For the η_C, the untreated device attenuates greatly at 0.8 V, however, the BzMIMBr modified device can maintain above 90% at 1.0 V, as presented in Fig. 4e. This result is further confirmed by admittance spectra (Fig. 4f). Extended equivalent circuit model is given to quantitatively extract the interface defect profile (Inset of Fig. 4f),[62, 63] specifically the interface defect density (N_{SS}). The N_{SS} of the BzMIMBr modified device is reduced from 9.46×10^{13} to 1.78×10^{13} cm^2 eV^{-1}, confirming effective interface passivation of the BzMIMBr incorporation. This reduction in interface defect density is consistent with its improved charge collection efficiency (η_C) from m-TPC/TPV, especially in the high voltage region, which is in good agreement of the V_{OC} and *FF* enhancement. Based on M-TPC/TPV results, the charge extraction efficiency (η_e) is estimated, which is enhanced particularly under high-voltage regime (Figure S15). This increase is primarily attributed to the BzMIMBr modification at the grain boundary, resulting in defect density decreased.

According to the above analysis, the passivation mechanism of BzMIMBr modification layer is proposed. On one hand, Br^- ions occupy the V_I (iodide vacancy) to give Pb-Br bonds, on the other hand, there is some weak coordination interaction between under-coordinated Pb^{2+} and N atom from $BzMIM^+$, both of which can significantly reduce the defects of the perovskite surface and suppress the Pb cluster formation. Besides, this passivation effect can further extend the bulk perovskite especially toward grain boundaries, due to good permeation of the BZMIMBr. Based on our previous work,[64] π-π conjugation may also occur between benzyl groups from neighboring $BzMIM^+$ cation at $FAPbI_3$/HTL modified interface, which also provide a kind of hydrophobicity layers to improve the water resistance of the perovskite films and the PSC device.

Finally, perovskite phase and cell efficiency stabilities under different aging conditions have been investigated. All samples whether perovskite films or PSCs for stability testing, are

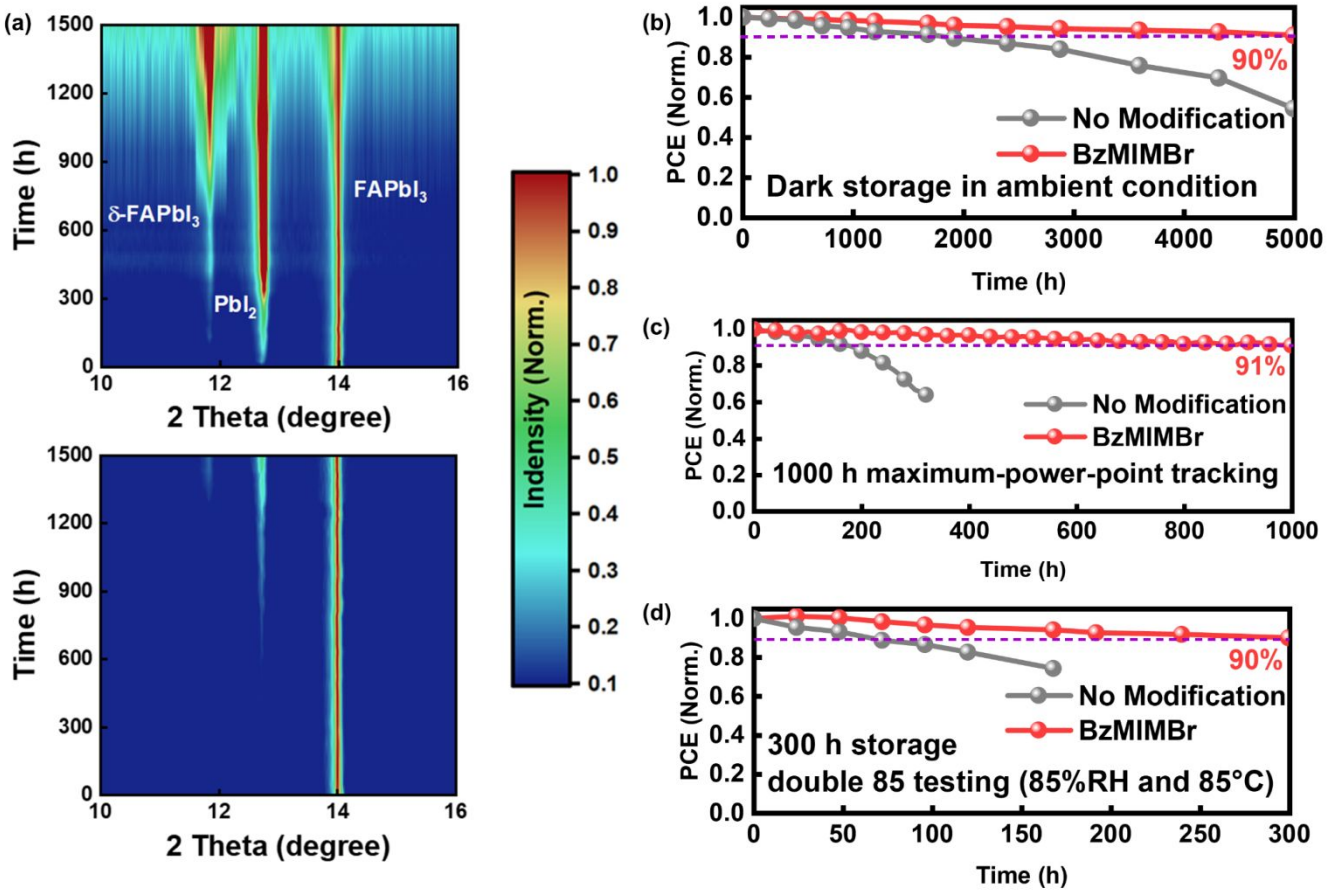

Fig. 5 (a) In situ X-ray diffraction pattern tracking of perovskite films with/without BzMIMBr modification aged in 60°C and 60%RH (relative humidity) for 500 h. (b) PCE tracking of non-encapsulated cells stored in ambient conditions (25°C and 20~30%RH) for 5000 h. (c) Operational stability tracking of cells under continuous light illumination and bias voltage near maximum power point for 1000 h (N_2 atmosphere, white LED). (d) PCE tracking of non-encapsulated cells stored under "double 85" testing in the air (85°C and 85%RH) for 300 h.

unpackaged. Firstly, the two perovskite films modified with or without BzMIMBr were kept under "double 60" testing condition (simultaneously at 60°C and 60%RH) for 1500 h, and variation process was monitored by XRD pattern tracking. It can be seen from Fig. 5a that, to the untreated perovskite film, its degradation appeared at the beginning with the appearance of the PbI_2 peak (typical 12.6º), when the testing time was extended to ~100 h, another characteristic peak at 11.8° corresponding to the photoinactive yellow δ-$FAPbI_3$ phase. However, to the BzMIMBr modified perovskite film, the characteristic diffraction peak of the δ-$FAPbI_3$ phase can be found only after ~1300 h, indicating excellent anti-humidity ability of $FAPbI_3$/BzMIMBr. The cells were kept under ambient conditions (~25°C, 20~30%RH) for 5,000 h. We can see that, BzMIMBr modified cells exhibit excellent long-term stability, which can maintain ~90% of their initial PCE after 5000 h, however, the efficiency of untreated devices dropped to 54% (Fig. 5b). Furthermore, the PSCs without and with BzMIMBr treatment exhibit different operational stability when being allowed to work under continuous light and steady-state bias voltage. Severe efficiency degradation was observed in the untreated cells after 200 h (Fig. 5c), however, no significant PCE degradation was found in BzMIMBr modified cells for comparison. After 1000 h operation, the modified cell can still maintain 91% of the initial PCE value. Also, "double 85" testing in the air (simultaneously at 85°C and 85%RH) was also performed to evaluate the stability of the cells in harsh environments (Fig. 5d). BzMIMBr modified cells can maintain 90% of the PCE value after 300 h, whereas the PCE of untreated cells was deteriorated significantly after 150 h due to their decomposition under high humidity. In short, the BzMIMBr incorporation on the perovskite surface can significantly enhance the phase stability of the perovskite itself and simultaneously is beneficial for the device stability due to interface defect passivation.

Conclusions

In our work, 1-methy-3-benzyl-limidazole halides (BzMIMX, X= I, Br, Cl) has been introduced on the perovskite/spiro-OMeTAD interface for efficient and stable PSCs. BzMIMBr exhibits the best cell performance, which PCE reaches 25.3% with negligible hysteresis. Passivation mechanism of BzMIMBr modification layer is also suggested. Firstly, Br^- ions occupy the V_I (iodide vacancy) and some weak coordination interaction between

under-coordinated Pb^{2+} and N atom from $BzMIM^{+}$, thus significantly reducing perovskite surface defects and preventing the Pb cluster formation. Secondly, the permeation of some BZMIMBr into the bulk perovskite can further passivate grain boundaries. Thirdly, π-π conjugation interaction between neighboring BzMIMBr molecules can improve the water resistance of the perovskite films and the PSC device. Thus, perovskite films exhibit good anti-humidity stability and "double 60" testing results. Besides, excellent long-term stability, operational MPP stability and "double 85" testing stability also confirm the excellent passivation effect of the BzMIMBr treatment towards PSC devices.

Author Contributions

Zijing Chen and Shiyu Jiang contributed equally to this work. Zijing Chen and Shiyu Jiang fabricated the devices, investigated and did some characterizations. Zijing Chen wrote original draft. Zhenghao Liu performed KPFM measurement and did data analysis. Jiangjian Shi, Yanhong Luo and Qingbo Meng analysed the data and discussed. Yiming Li performed admittance spectra, m-TPC/TPV measurements and discussed. Huijue Wu supported the characterizations. Dongmei Li and Qingbo Meng supervised, participated in reviewing the manuscript. All authors were involved in the discussions and approved the manuscript.

Conflicts of interest

There are no conflicts of interest to declare.

Acknowledgements

We would like to thank the financial support from Natural Science Foundation of China (Nos. 52102332, 52072402, 52203368, 52172260, 52227803, 52222212), the Ministry of Science and Technology of China (2021YFB3800103), Beijing Natural Science Foundation (2222082), CAS-CSIRO Joint Project (112111KYSB20210017).

References

1. J. Park, J. Kim, H.-S. Yun, M. J. Paik, E. Noh, H. J. Mun, M. G. Kim, T. J. Shin and S. I. Seok, *Nature*, 2023, **616**, 724-730.
2. J. Zhou, L. Tan, Y. Liu, H. Li, X. Liu, M. Li, S. Wang, Y. Zhang, C. Jiang, R. Hua, W. Tress, S. Meloni and C. Yi, *Joule*, 2024, DOI: 10.1016/j.joule.2024, **02**, 019.
3. Y. Zheng, Y. Li, R. Zhuang, X. Wu, C. Tian, A. Sun, C. Chen, Y. Guo, Y. Hua, K. Meng, K. Wu and C.-C. Chen, *Energy Environ. Sci.*, 2024, **17**, 1153-1162.
4. H. Zhang, L. Pfeifer, S. M. Zakeeruddin, J. Chu and M. Grätzel, *Nat. Rev. Chem.*, 2023, **7**, 632-652.
5. J. W. Yoo, E. Noh, J. Jang, K. S. Lee, J. Byeon, M. Choi, J. Im and S. I. Seok, *Joule*, 2023, **7**, 797-809.
6. X. Wei, M. Xiao, B. Wang, C. Wang, Y. Li, J. Dou, Z. Cui, J. Dou, H. Wang, S. Ma, C. Zhu, G. Yuan, N. Yang, T. Song, H. Zhou, H. Chen, Y. Bai and Q. Chen, *Angew. Chem. Int. Ed.*, 2022, **61**, 27
7. Y. Li, Z. Chen, B. Yu, S. Tan, Y. Cui, H. Wu, Y. Luo, J. Shi, D. Li and Q. Meng, *Joule*, 2022, **6**, 676-689.
8. A. J. Ramadan, R. D. J. Oliver, M. B. Johnston and H. J. Snaith, *Nat. Rev. Mater.* 2023, **8**, 822-838.
9. X. Shen, B. M. Gallant, P. Holzhey, J. A. Smith, K. A. Elmestekawy, Z. Yuan, P. V. G. M. Rathnayake, S. Bernardi, A. Dasgupta, E. Kasparavicius, T. Malinauskas, P. Caprioglio, O. Shargaieva, Y. H. Lin, M. M. McCarthy, E. Unger, V. Getautis, A. Widmer-Cooper, L. M. Herz and H. J. Snaith, *Adv. Mater.*, 2023, **35**, 2211742.
10. D.-H. Kang, C. Ma and N.-G. Park, *ACS Appl. Mater. Interfaces*, 2022, **14**, 8984-8991.
11. Z. Huang, Y. Bai, X. Huang, J. Li, Y. Wu, Y. Chen, K. Li, X. Niu, N. Li, G. Liu, Y. Zhang, H. Zai, Q. Chen, T. Lei, L. Wang and H. Zhou, *Nature*, 2023, **623**, 531-537.
12. K. X. Steirer, P. Schulz, G. Teeter, V. Stevanovic, M. Yang, K. Zhu and J. J. Berry, *ACS Energy lett.*, 2016, **1**, 360-366.
13. C. Eames, J. M. Frost, P. R. F. Barnes, B. C. O'Regan, A. Walsh and M. S. Islam, *Nat. Commun.*, 2015, **6**, 7497
14. Z. Y. Ni, C. X. Bao, Y. Liu, Q. Jiang, W. Q. Wu, S. S. Chen, X. Z. Dai, B. Chen, B. Hartweg, Z. S. Yu, Z. Holman and J. S. Huang, *Science*, 2020, **367**, 1352-1358.
15. M. Xiao, G. Yuan, Z. Lu, J. Xia, D. Li, Y. Chen, Y. Zhang, F. Pei, C. Chen, Y. Bai, T. Song, J. Dou, Y. Li, Y. Chen, Z. Xu, X. Yang, Z. Liu, X. Liu, C. Zhu and Q. Chen, *Adv. Mater.*, 2023, **35**, 2301684.
16. J. Dou, Y. Ma, X. Niu, W. Zhou, X. Wei, J. Dou, Z. Cui, Q. Song, T. Song, H. Zhou, C. Zhu, Y. Bai and Q. Chen, *J. Energy Chem.*, 2024, **88**, 64-70.
17. A. Maxwell, H. Chen, L. Grater, C. Li, S. Teale, J. Wang, L. Zeng, Z. Wang, S. M. Park, M. Vafaie, S. Sidhik, I. W. Metcalf, Y. Liu, A. D. Mohite, B. Chen and E. H. Sargent, *ACS Energy Lett.*, 2024, **9**, 520-527.
18. Z. Shen, Q. Han, X. Luo, Y. Shen, Y. Wang, Y. Yuan, Y. Zhang, Y. Yang and L. Han, *Nat. Photonics*, 2024, DOI: 10.1038/s41566-024-01383-5.
19. S. Tan, B. Yu, Y. Cui, F. Meng, C. Huang, Y. Li, Z. Chen, H. Wu, J. Shi, Y. Luo, D. Li and Q. Meng, *Angew. Chem. Int. Ed.* 2022, **61**, e202201300.
20. M. Almalki, M. H. Alotaibi, A. Q. Alanazi, F. T. Eickemeyer, S. M. Alenzi, Y. A. Alzahrani, L. Piveteau, A. Y. Alymani, A. Albadri, H. Albrithen, J. V. Milić, S. M. Zakeeruddin, H. Zhang and M. Grätzel, *Adv. Funct. Mater.*, 2023, **34(6)**, 2309789
21. J. Xu, A. Maxwell, Z. Song, A. S. R. Bati, H. Chen, C. Li, S. M. Park, Y. Yan, B. Chen and E. H. Sargent, *Nat. Commun.*, 2024, **15(1)**, 2035
22. X. Chu, Q. Ye, Z. Wang, C. Zhang, F. Ma, Z. Qu, Y. Zhao, Z. Yin, H.-X. Deng, X. Zhang and J. You, *Nat. Energy*, 2023, **8**, 372-380.
23. K. Sun, Y. Meng, R. Cao, Y. Ren, Y. Mao, R. Tian, Y. Wang, X. Lü, C. Liu and Z. Ge, *J. Mater. Chem. A*, 2024, **12**, 5215-5224.
24. W. Zhang, T. Zhang, L. Qin, S.-Z. Kang, Y. Zhao and X. Li, *Chem. Eng. J.*, 2024, **479**, 147838.
25. Y. Miao, M. Ren, Y. Chen, H. Wang, H. Chen, X. Liu, T. Wang and Y. Zhao, *Nat. Sustainability*, 2023, **6**, 1465-1473.
26. S. Yu, Z. Xiong, H. Zhou, Q. Zhang, Z. Wang, F. Ma, Z. Qu, Y. Zhao, X. Chu, X. Zhang and J. You, *Science*, 2023, **382**, 1399-1404.
27. P. Dong, B. Chen, D. Yao, S. Li, J. Su, B. Zhou, N. Tian, G. Zheng, Y. Peng and F. Long, *J. Mater. Chem. A*, 2024, **12**, 6134-6145.
28. Q. Hu, K. Zhao, M. Liu, S. Riaz, Y. Qi, P. Wei, J. Cheng and Y. Xie, *J. Mater. Chem. A*, 2024, **12**, 5980-5989.
29. W. Zhou, D. Li, Z. Xiao, Z. Wen, M. Zhang, W. Hu, X. Wu, M. Wang, W. H. Zhang, Y. Lu, S. Yang and S. Yang, *Adv. Funct. Mater.*, 2019, **29**, 23
30. L. Chen, L. Chen, Z. Chen, J. Wu, T. Lou, Y. Li, Z. Zhou, H. Li, G. Li and Q. Meng, *Small*, 2024, DOI: 10.1002/smll.202308964.
31. N. Ahn, D.-Y. Son, I.-H. Jang, S. M. Kang, M. Choi and N.-G. Park, *J. Am. Chem. Soc.*, 2015, **137**, 8696-8699.
32. Q. Jiang, Y. Zhao, X. Zhang, X. Yang, Y. Chen, Z. Chu, Q. Ye, X. Li, Z. Yin and J. You, *Nat. Photonics*, 2019, **13**, 460-466.
33. J. H. Heo, H. J. Han, D. Kim, T. K. Ahn and S. H. Im, *Energy Environ. Sci.*, 2015, **8**, 1602-1608.

34. D. Bi, C. Yi, J. Luo, J.-D. Décoppet, F. Zhang, Shaik M. Zakeeruddin, X. Li, A. Hagfeldt and M. Grätzel, *Nat. Energy*, 2016, **1**, 16142.
35. Y. Shao, Z. Xiao, C. Bi, Y. Yuan and J. Huang, *Nat. Commun.*, 2014, **5**, 5784.
36. J. Xu, A. Buin, A. H. Ip, W. Li, O. Voznyy, R. Comin, M. Yuan, S. Jeon, Z. Ning, J. J. McDowell, P. Kanjanaboos, J. P. Sun, X. Lan, L. N. Quan, D. H. Kim, I. G. Hill, P. Maksymovych and E. H. Sargent, *Nat. Commun.*, 2015, **6**, 7081.
37. J. Wang, K. Datta, C. H. L. Weijtens, M. M. Wienk and R. A. J. Janssen, *Adv. Funct. Mater.*, 2019, **29**, 1905883.
38. Y. Dong, W. Li, X. Zhang, Q. Xu, Q. Liu, C. Li and Z. Bo, *Small*, 2016, **12**, 1098-1104.
39. Z. Chen, Y. Li, Z. Liu, J. Shi, B. Yu, S. Tan, Y. Cui, C. Tan, F. Tian, H. Wu, Y. Luo, D. Li and Q. Meng, *Adv. Energy Mater.*, 2022, **13**, 2202799.
40. J. Kim, T. Hwang, B. Lee, S. Lee, K. Park, H. H. Park and B. Park, *Small Methods*, 2019, **3**, 1800361.
41. S. Yu, J. Meng, Q. Pan, Q. Zhao, T. Pullerits, Y. Yang, K. Zheng and Z. Liang, *Energy Environ. Sci.*, 2022, **15**, 3321-3330.
42. S. Huang, G. Dong, L. Zhu and B. Guan, *ChemSusChem*, 2023, **16**, 24
43. J. Xu, J. Cui, S. Yang, Y. Han, X. Guo, Y. Che, D. Xu, C. Duan, W. Zhao, K. Guo, W. Ma, B. Xu, J. Yao, Z. Liu and S. Liu, *Nano-micro lett.*, 2021, **14**, 1
44. D. B. Khadka, Y. Shirai, M. Yanagida, H. Ota, A. Lyalin, T. Taketsugu and K. Miyano, *Nat. Commun.*, 2024, **15**, 1
45. I. B. Abdul Ghani, M. Khalid, M. I. Hussain, M. M. Hussain, R. Ashraf and J. Wang, *Mater. Sci. Semicond. Process.*, 2022, **148**, 106788.
46. J. J. Yoo, G. Seo, M. R. Chua, T. G. Park, Y. Lu, F. Rotermund, Y.-K. Kim, C. S. Moon, N. J. Jeon, J.-P. Correa-Baena, V. Bulović, S. S. Shin, M. G. Bawendi and J. Seo, *Nature*, 2021, **590**, 587-593.
47. N. Li, S. Tao, Y. Chen, X. Niu, C. K. Onwudinanti, C. Hu, Z. Qiu, Z. Xu, G. Zheng, L. Wang, Y. Zhang, L. Li, H. Liu, Y. Lun, J. Hong, X. Wang, Y. Liu, H. Xie, Y. Gao, Y. Bai, S. Yang, G. Brocks, Q. Chen and H. Zhou, *Nat. Energy*, 2019, **4**, 408-415.
48. J. Xu, A. Maxwell, M. Wei, Z. Wang, B. Chen, T. Zhu and E. H. Sargent, *ACS Energy lett.*, 2021, **6**, 4220-4227.
49. M. Kim, G.-H. Kim, T. K. Lee, I. W. Choi, H. W. Choi, Y. Jo, Y. J. Yoon, J. W. Kim, J. Lee, D. Huh, H. Lee, S. K. Kwak, J. Y. Kim and D. S. Kim, *Joule*, 2019, **3**, 2179-2192.
50. T. Singh and T. Miyasaka, *Adv. Energy Mater.*, 2018, **8**, 1700677.
51. J. Burschka, N. Pellet, S. J. Moon, R. Humphry-Baker, P. Gao, M. K. Nazeeruddin and M. Grätzel, *Nature*, 2013, **499**, 316-319.
52. H. Min, M. Kim, S.-U. Lee, H. Kim, G. Kim, K. Choi, J. H. Lee and S. I. Seok, *Science*, 2019, **366**, 749-753.
53. J. Jeong, M. Kim, J. Seo, H. Lu, P. Ahlawat, A. Mishra, Y. Yang, M. A. Hope, F. T. Eickemeyer, M. Kim, Y. J. Yoon, I. W. Choi, B. P. Darwich, S. J. Choi, Y. Jo, J. H. Lee, B. Walker, S. M. Zakeeruddin, L. Emsley, U. Rothlisberger, A. Hagfeldt, D. S. Kim, M. Grätzel and J. Y. Kim, *Nature*, 2021, **592**, 381-385.
54. L. Wang, H. Zhou, J. Hu, B. Huang, M. Sun, B. Dong, G. Zheng, Y. Huang, Y. Chen, L. Li, Z. Xu, N. Li, Z. Liu, Q. Chen, L.-D. Sun and C.-H. Yan, *Science*, 2019, **363**, 265-270.
55. R. Wang, M. Mujahid, Y. Duan, Z. K. Wang, J. Xue and Y. Yang, *Adv. Funct. Mater.*, 2019, **29**, 1808843.
56. Y. Zhao, F. Ma, Z. Qu, S. Yu, T. Shen, H.-X. Deng, X. Chu, X. Peng, Y. Yuan, X. Zhang and J. You, *Science*, 2022, **377**, 531-534.
57. Z. Wang, J. Wang, S. Zhu, T. Ma, M. Zhang and M. Guo, *ACS Sustainable Chem. Eng.*, 2023, **11**, 14559-14571.
58. J. Shi, Y. Li, Y. Li, D. Li, Y. Luo, H. Wu and Q. Meng, *Joule*, 2018, **2**, 879-901.
59. J. Shi, D. Li, Y. Luo, H. Wu and Q. Meng, *Rev. Sci. Instrum.*, 2016, **87**, 123107.
60. Y. M. Li, J. J. Shi, H. J. Wu, Y. H. Luo, D. M. Li and Q. B. Meng, *Sci. Chin. Mater.*, 2021, **64**, 61-72.
61. Y. Li, J. Shi, B. Yu, B. Duan, J. Wu, H. Li, D. Li, Y. Luo, H. Wu and Q. Meng, *Joule*, 2020, **4**, 472-489.
62. B. Yu, J. Shi, S. Tan, Y. Cui, W. Zhao, H. Wu, Y. Luo, D. Li and Q. Meng, *Angew. Chem. Int. Ed.*, 2021, **60**, 13436.
63. Y. Cui, J. Shi, F. Meng, B. Yu, S. Tan, S. He, C. Tan, Y. Li, H. Wu, Y. Luo, D. Li and Q. Meng, *Adv. Mater.*, 2022, **34**, 2205028.
64. H. Li, J. J. Shi, J. Deng, Z. J. Chen, Y. M. Li, W. Y. Zhao, J. H. Wu, H. J. Wu, Y. H. Luo, D. M. Li and Q. B. Meng, *Adv. Mater.*, 2020, **32**, 1907356.